Electronic Research Archive

https://www.aimspress.com/journal/era

ERA, 34(4): 2402–2418.
DOI: 10.3934/era.2026110
Received: 29 January 2026
Revised: 07 March 2026
Accepted: 13 March 2026
Published: 19 March 2026

Research article

Effect of the striatum on β-synchronous oscillatory activity

Quanbao Ji[1,2] **and Ruhu Lao**[1,*]

[1] School of Mathematical Sciences, Guangxi Minzu University, Nanning 530006, China

[2] Guangxi Key Laboratory of Universities Optimization Control and Engineering Calculation, Nanning 530006, China

* **Correspondence:** Email:lrh201621@163.com.

Abstract: Parkinson's disease (PD) is characterized by increased β-band (13–30 Hz) synchronization. Although previous studies have indicated that the striatum plays a crucial part in generating and transmitting the β-band oscillations, the underlying biophysical basis remains unclear. An extended thalamic–basal ganglia (BGTC) model including the striatum (BGSTC) is used to examine the striatal influence on β-band synchronous oscillations in the globus pallidus pars interna (GPi). This influence is implemented by modulating striatal inhibitory input. Phase-locking value (PLV) and phase consistency (PC) show that the basal ganglia (BG) network exhibits pronounced β-band synchrony in the Parkinsonian state. Moreover, enhancing striatal synaptic inputs may induce β-band desynchronization in GPi via the direct pathway. In contrast, the modulation via the indirect pathway has a much weaker influence and may even exert an opposite effect. These conclusions not only reveal the striatum's regulatory capacity, but also provide a new avenue for PD therapy.

Keywords: Parkinson's disease; β-band synchrony; striatum; phase-locking value; phase consistency

1. Introduction

A hallmark of Parkinson's disease (PD) is increased β-band oscillatory activity within the basal ganglia (BG), which presents as aberrant synchronization [1]. The pathological β-band synchrony is closely linked to PD motor impairments, including rigidity and bradykinesia [2]. As a major output node of the BG, globus pallidus pars interna (GPi) serves as a key regulator of information exchange between the thalamus (TC) and the sensorimotor cortex [3]. The aberrant synchrony may compromise thalamic relaying of motor commands [4,5]. The striatum, a potential source of oscillations, contributes critically to generating and transmitting β-band rhythms [6]. It is primarily composed of medium spine neurons (MSNs) in the striatum expressing dopamine D1 receptors (D1 MSNs) and D2 receptors (D2 MSNs), fast-spiking interneurons (FSIs). Additionally, D1 MSNs and GPi form the direct pathway,

whereas D2 MSNs, globus pallidus pars externa (GPe), subthalamic nucleus (STN), and GPi constitute the indirect pathway [7]. The direct pathway that is driven by D1 MSNs tends to facilitate movement, whereas the indirect pathway, driven by D2 MSNs, suppresses it [8]. Therefore, research on how the striatum modulates the β-band synchrony in GPi neurons will contribute to advancing PD research via the direct and indirect pathways. However, the relevant mechanisms still need further study.

Many computational models used to study the activities of neural networks are constantly being improved and developed. The basal ganglia thalamocortical circuit (BGTC) network model was introduced by Terman and Rubin [4]. So et al. later refined the BGTC model by adjusting the number of neurons and synaptic network topology [9]. However, the refined BGTC model did not consider the striatum's contribution to network dynamics. Although Van Albada et al. introduced the mean-field model including the striatum, it still did not adequately account for striatum microcirculation [10]. Gittis et al. built a striatal neural circuit network model and systematically investigated how the striatum influences pathological network synchrony and oscillatory activity through the direct and indirect pathways [11]. McCarthy et al. demonstrated that striatum can generate the β-band oscillations [6]. Corbit et al. modeled the GPe–FSI–MSN circuit, demonstrating that it can also generate β-band oscillations, and studied the influence of connections on the generation of synchronization [12]. Most of the studies on the pathological β-band synchrony in PD heve focused on the subthalamic nucleus (STN)–GPe loop or treated striatal input as fixed, whereas the regulatory role of the striatum on GPi has been less explored.

This study aims to investigate the modulatory role of the striatum in pathological β-band oscillations in PD. Specifically, it examines how inhibitory striatal inputs via the direct and indirect pathways affect synchrony in the BG output nucleus (GPi). To address this, the basal ganglia–striatum thalamocortical circuit (BGSTC) computational model is used, combined with existing experimental data, to explore β-band oscillatory activity in the BG in PD. Using phase-locking value (PLV) [13, 14] and phase consistency (PC) [15] as metrics of synchrony, this study systematically evaluates the impact of changes in striatal inhibitory synaptic conductance on the synchrony of GPi in the β-band. This provides a new perspective for a deeper understanding of the role of the striatum in PD, particularly in the modulation of pathological β-band oscillations.

2. Materials and methods

The BGTC model, improved by So et al. [9], consists of four interacting nuclei: STN, GPe, GPi, and TC. The dynamic equations are as follows:

$$\begin{aligned}
C_m\frac{dV_{TC}}{dt} &= -I_L - I_{Na} - I_K - I_T - I_{GPi\to TC} + I_{SMC},\\
C_m\frac{dV_{STN}}{dt} &= -I_L - I_{Na} - I_K - I_T - I_{Ca} - I_{AHP} - I_{GPe\to STN} + I^{STN}_{app},\\
C_m\frac{dV_{GPe}}{dt} &= -I_L - I_{Na} - I_K - I_T - I_{Ca} - I_{AHP} - I_{STN\to GPe} - I_{GPe\to GPe} - I_{D2\to GPe} + I^{GPe}_{app},\\
C_m\frac{dV_{GPi}}{dt} &= -I_L - I_{Na} - I_K - I_T - I_{Ca} - I_{AHP} - I_{STN\to GPi} - I_{GPe\to Gpi} - I_{D1\to GPi} + I^{GPi}_{app},
\end{aligned} \tag{2.1}$$

where C_m denotes membrane capacitance, I_{Na} represents the sodium current, I_K denotes the potassium current, I_L represents the leakage current, I_T denotes the low-threshold T-calcium current, I_{Ca} represents the calcium current, I_{AHP} represents the calcium-activated potassium current, and I_{SMC} is the cortical sensorimotor signal.

The striatum microcirculation is composed of D1 MSNs, D2 MSNs, and FSIs. The specific dynamic equations are as follows:

$$\begin{aligned} C_m\frac{dV_{D1}}{dt} &= -I_L - I_{Na} - I_K - I_M - I_{CaL1.3} - I_{kir} - I_{FSI\to D1} - I_{D1\to D1} - I_{D2\to D1} + I_{app}^{D1}, \\ C_m\frac{dV_{D2}}{dt} &= -I_L - I_{Na} - I_K - I_M - I_{CaL1.3} - I_{kir} - I_{FSI\to D2} - I_{D2\to D2} - I_{D1\to D2} + I_{app}^{D2}, \\ C_m\frac{dV_{FSI}}{dt} &= -I_L - I_{Na} - I_K - I_{FSI\to FSI} + I_{app}^{FSI}, \end{aligned} \tag{2.2}$$

where I_M denotes the M-current, I_{Kir} represents the Kir current, and I_{CaL} represents the L-type Ca^{2+}(CaL1.3) current. According to the study by So et al. [9], the BGSTC network model is coupled via chemical synapses. The synaptic current $I_{\alpha\to\beta}$ is defined as follows:

$$I_{\alpha\to\beta} = g_{\alpha\to\beta}(V_\beta - V_{\alpha\to\beta})\sum_k s_\alpha^k, \tag{2.3}$$

where $g_{\alpha\to\beta}$ represents the synaptic conductance. $V_{\alpha\to\beta}$ denotes the synaptic reversal potential, and s_α^k corresponds to the synaptic gating variable associated with the kth presynaptic neuron [9]. It is defined as follows:

$$\begin{aligned} &\frac{ds}{dt} = 2(1-s)H_\infty(V-20) - 0.04s, \\ &H_\infty(V) = 1/(1+exp(-(V+57)/2)). \end{aligned} \tag{2.4}$$

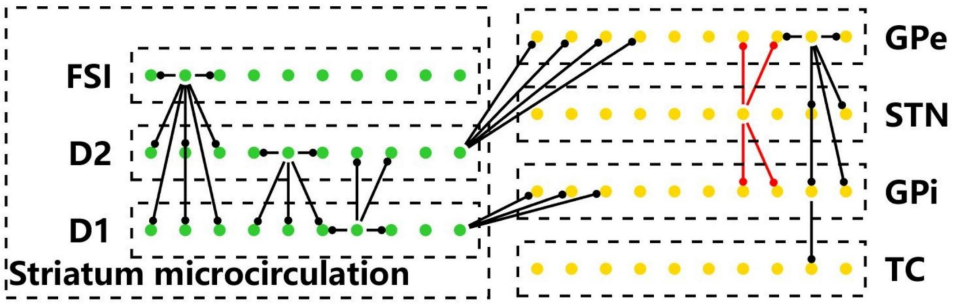

(a) (b)

Figure 1. Network architecture of the BGSTC model. (a) Striatal microcircuit and its projections to downstream nuclei. (b) Connectivity of the BGTC loop. The red lines represent positive effects, and the black ones represent inhibitory effects.

To enhance the sensitivity of synapses in STN and GPi neurons, the alpha synapse is adopted [9]. The synaptic gating variable s is governed by the following second-order differential equation:

$$\begin{aligned} \frac{ds}{dt} &= z, \\ \frac{dz}{dt} &= 0.234 Heaviside(V + 10) - 0.4z - 0.04s. \end{aligned} \tag{2.5}$$

Experimental evidence indicates that synaptic coupling from D2 MSNs to D1 MSNs is stronger than that from D1 MSNs to D2 MSNs and that inhibitory projections from FSIs to D1 MSNs are stronger than those to D2 MSNs [16]. In addition, the synaptic conductance parameters associated with the striatal microcircuit are adopted from a previously established extended BGTC computational framework [17], which are summarized in Table 1. The remaining parameters can be found in the work of So et al. [9].

Table 1. Synaptic parameters.

Synaptic conductance	Value (mS/cm^2)	Synaptic conductance	Value (mS/cm^2)
$g_{D1\to D1}$	0.05	$g_{D2\to D1}$	0.05
$g_{D1\to D2}$	0.02	$g_{D2\to D2}$	0.03
$g_{D1\to GPi}$	0.1	$g_{D2\to GPe}$	0.1
$g_{FSI\to D1}$	0.11	$g_{FSI\to D2}$	0.08
$g_{FSI\to FSI}$	0.1		

Within the BGSTC framework, each nucleus comprises 10 neurons, which are connected in a sparse yet structured manner as described in the literature [17]. A periodic boundary condition is imposed such that the first neuron is treated as adjacent to the 10th. Moreover, each neuron sequentially receives input from and projects to its nearest neighboring neurons. For example, the ith STN receives inhibitions from the $(i-1)$th and ith GPe and then sends excitatory projections to the ith and $(i+1)$th neurons in both GPe and GPi (see Figure 1).

3. Results

3.1. Electrophysiological properties

The I_{app} values used to define the healthy and Parkinsonian states are adopted based on the BGTC modeling framework established by So et al. [9] and can reproduce the abnormal firing characteristics of the neuronal populations. The specific values are provided in Table 2.

Table 2. Applied currents to BG under healthy and Parkinsonian conditions.

Conditions	I_{app}^{STN}	I_{app}^{GPe}	I_{app}^{GPi}
Healthy	$33\mu A/cm^2$	$22\mu A/cm^2$	$21\mu A/cm^2$
Parkinsonian	$23\mu A/cm^2$	$8\mu A/cm^2$	$16\mu A/cm^2$

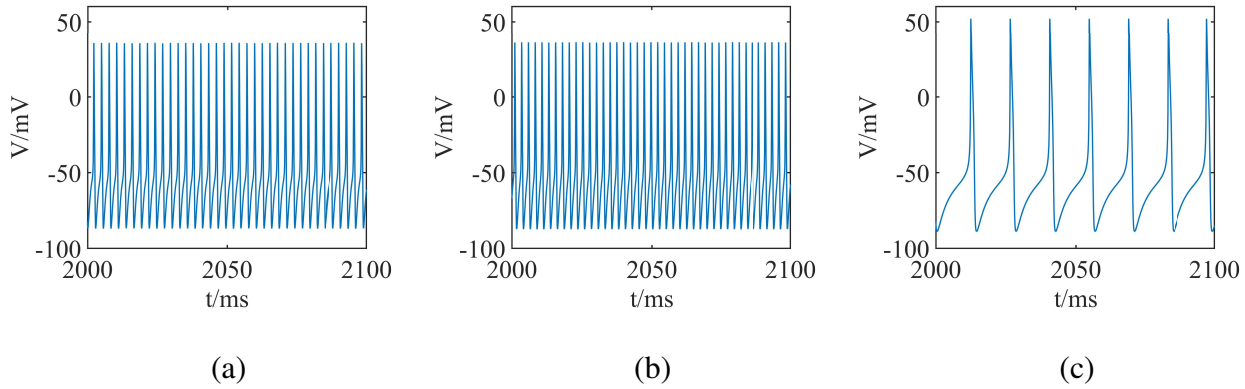

Figure 2. Membrane potential of striatal neurons under the specified model parameters. (a) D1 MSN ($I_{app}^{D1} = 6\mu A/cm^2$). (b) D2 MSN ($I_{app}^{D2} = 5.5\mu A/cm^2$). (c) FSI ($I_{app}^{D1} = 5\mu A/cm^2$).

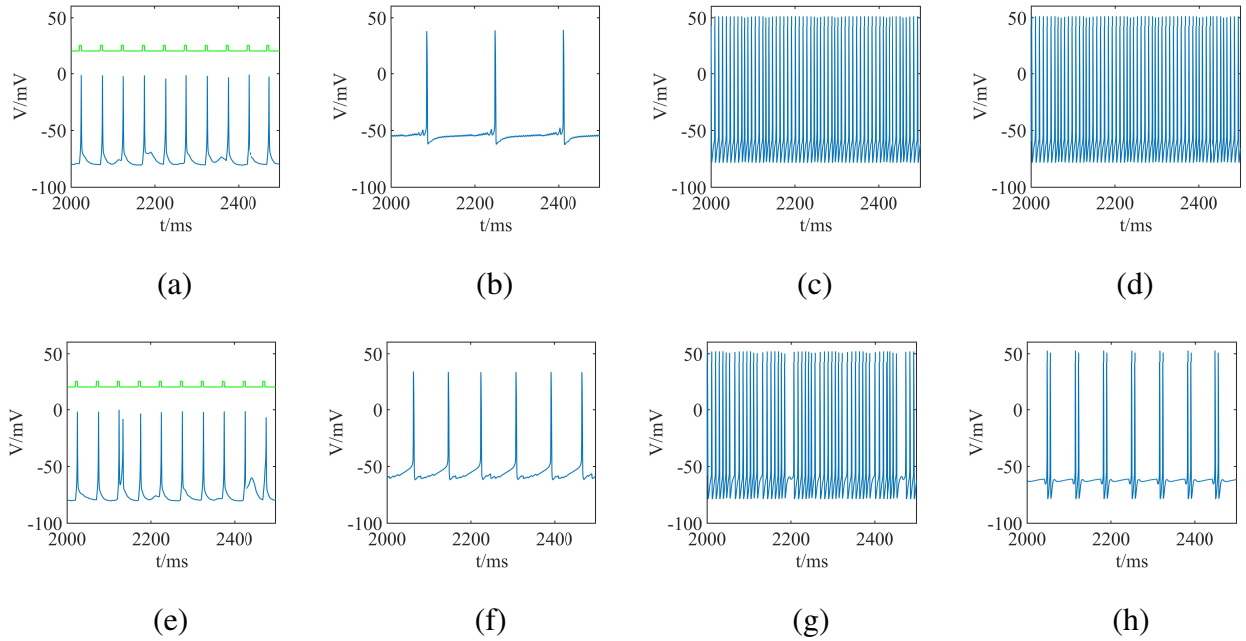

Figure 3. Membrane potential of individual neurons under different conditions. The green lines represent the sensorimotor cortical input signal. (a) TC in healthy condition. (b) STN in healthy condition. (c) GPi in healthy condition. (d) GPe in healthy condition. (e) TC in PD. (f) STN in PD. (g) GPi in PD. (h) GPe in PD.

Figure 2 shows the electrical activities of FSI, D1 MSN, and D2 MSN. They all exhibit continuous high-frequency firing, with D2 MSN firing at a slightly higher rate than D1 MSN. Figures 3(a),(e) depict thalamic responses to sensorimotor cortical input. The results indicate that, in the Parkinsonian state, thalamic responses shift from complete responses to response failures. This may lead to symptoms such as bradykinesia and resting tremor [18]. Figures 3(b),(f) indicate that the STN firing rate is mildly elevated in PD. Figures 3(c),(d),(g),(h) show the electrical activities of GPi and GPe under

healthy and Parkinsonian conditions, indicating that burst firing in both nuclei is markedly increased in the pathological state.

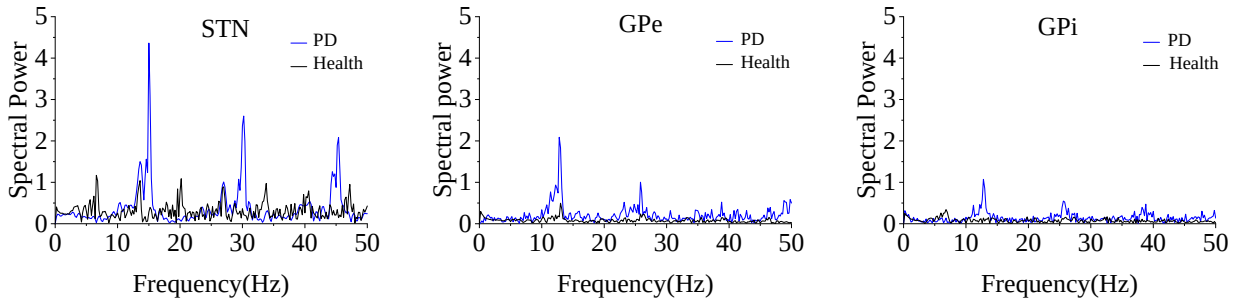

Figure 4. The spectral power of neurons in different states. The black trace denotes the healthy condition, and the blue trace represents the Parkinsonian condition. (a) STN. (b) GPe. (c) GPi.

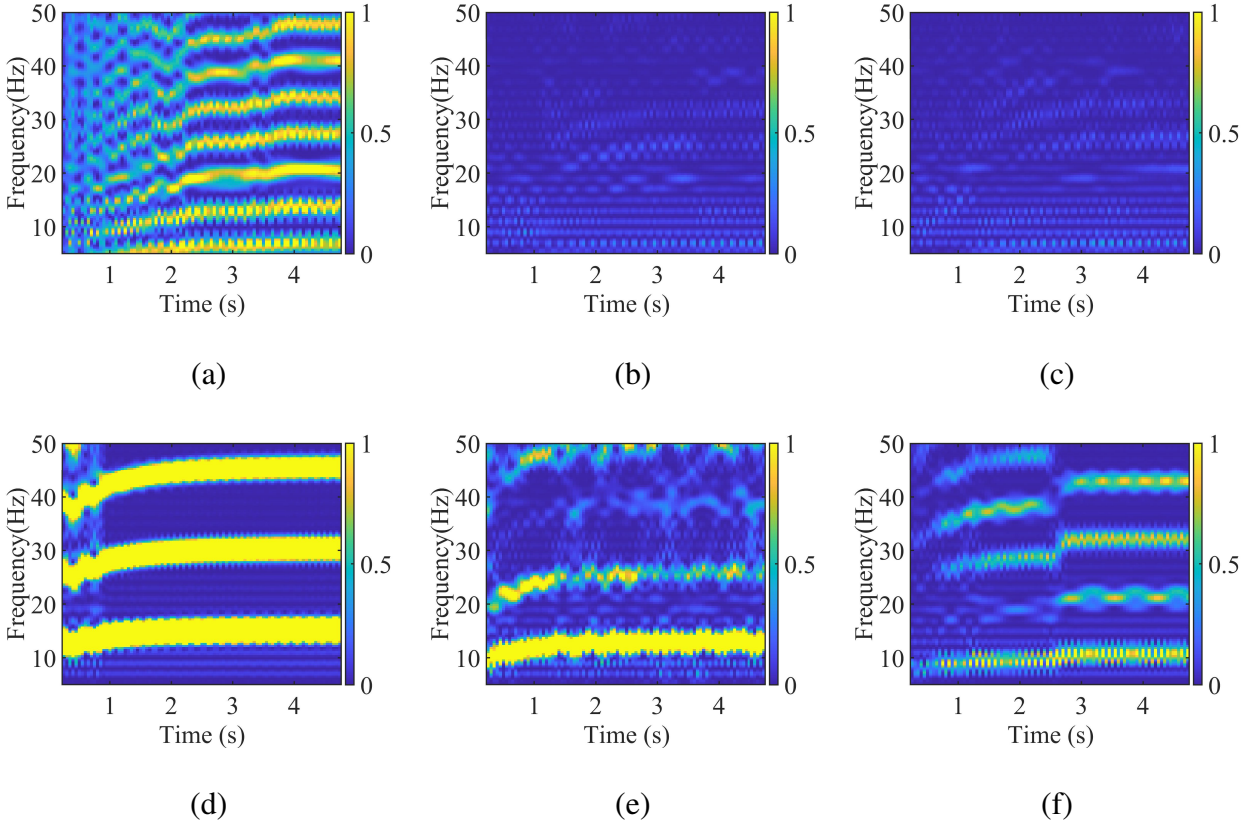

Figure 5. Spectral diagrams of neurons in the BGTC model under different conditions. (a) STN in healthy condition. (b) GPe in healthy condition. (c) GPi in healthy condition. (d) STN in PD. (e) GPe in PD. (f) GPi in PD.

Abnormal oscillations in the BG are the hallmark pathological feature of PD, such as β-band oscillations [19, 20]. To further investigate β-band oscillations, power spectral analyses are performed. In Figure 4(a), some pronounced spectral peaks appear in the 13–30 Hz range, indicating that STN exhibits strong β-band oscillatory activity under Parkinsonian conditions. As shown in Figures 4(b),(c), the β-band peaks of GPe and GPi are lower than those of STN in the Parkinsonian state, yet they are clearly elevated relative to the healthy condition.

Additionally, Figure 5(a) shows that, in the healthy condition, the STN spectrogram exhibits β-band stripes that are intermittent and scattered. In contrast, under Parkinsonian conditions (see Figure 5(d)), the β-band displays stable, narrow stripes, indicating a marked increase in β-power and rhythmicity. Figures 5(b),(c) indicate that the β-band oscillations in GPe and GPi are not prominent. By comparison, in Figures 5(e),(f), sustained and layered narrowband β-band stripes are observed, indicating that β-band power and rhythmicity are markedly enhanced in both neurons under Parkinsonian conditions. Overall, under Parkinsonian conditions, all three nuclei exhibit a pronounced increase in β-band power and persistence, with STN showing the strongest effect and GPe and GPi comparatively weaker.

3.2. Phase synchronization

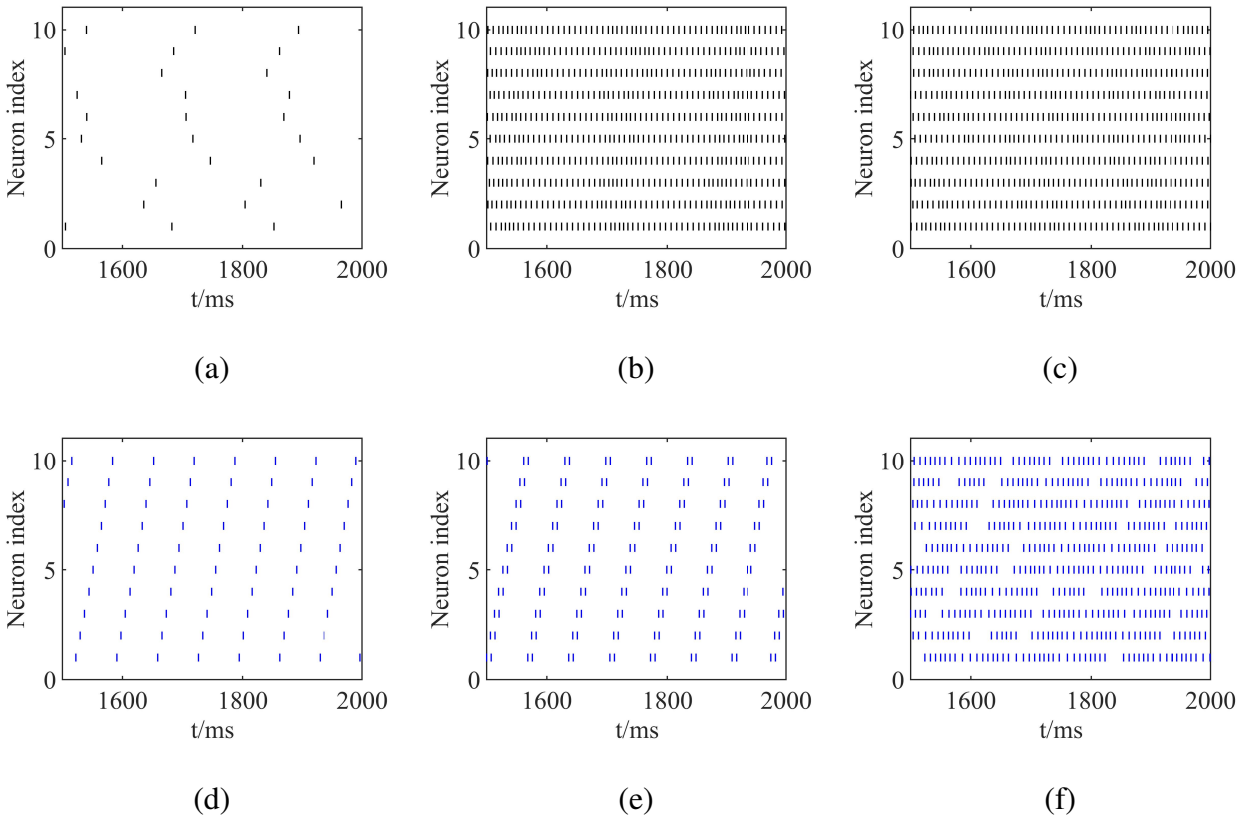

Figure 6. Firing peak diagrams. (a) STN in healthy condition. (b) GPe in healthy condition. (c) GPi in healthy condition. (d) STN in PD. (e) GPe in PD. (f) GPi in PD.

The increase in the β-band oscillations typically manifests as abnormal synchrony [21, 22]. As shown in Figures 6(a)–(c), in the healthy state, these three neuronal populations exhibit stochastic firing patterns. In Figure 6(d), the STN spike trains become denser and more regular. Besides, the spike trains of GPe and GPi exhibit more pronounced regularity and clear burst firing (see Figures 6(e),(f)). These results reveal a clear enhancement of synchronization in the BG under Parkinsonian conditions.

In order to better study the β-band synchrony of the BG, several quantitative indicators are explained here. The local field potential (LFP) provides a useful measure for quantifying clinically relevant symptoms in diverse neurological conditions [23]. It serves as a key feedback signal for neural regulation and control [24].

The LFP can be modeled as follows [25]:

$$LFP = -I_{syn} + Iapp, \tag{3.1}$$

where I_{syn} denotes the total synaptic current. $I_{GPe_{syn}}$ received by the ith GPe is expressed as follows:

$$\begin{aligned} I_{GPe_{syn}} &= I_{GPe\to GPe} + I_{STN\to GPe} + I_{D2\to GPe}, \\ &= g_{GPe\to GPe}(V^i_{GPe} - V_{GPe\to GPe}) \cdot (s^{i-1}_{GPe} + s^{i+1}_{GPe}) \\ &+ g_{STN\to GPe}(V^i_{GPe} - V_{STN\to GPe}) \cdot (s^{i}_{STN} + s^{i+1}_{STN}) \\ &+ g_{D2\to GPe}(V^i_{GPe} - V_{D2\to GPe}) \cdot (s^{i-1}_{D2} + s^{i}_{D2} + s^{i+1}_{D2} + s^{i+2}_{D2}), \end{aligned} \tag{3.2}$$

where i represents the index of the neuron within the population of a given nucleus. Additionally, the subsequent analyses are performed using the LFP.

In the dataset created by Biswas and Ananna [26], which contains electrophysiological signals from healthy and Parkinsonian conditions, the STN LFP is available. Figures 7(a),(d) show the LFP curves of STN under different conditions. The curves indicate that, under Parkinsonian conditions, the LFP signals exhibit higher amplitudes and more sustained fluctuations. It suggests the presence of relatively stable low-frequency oscillations. Figures 7(b),(e) show the power spectra, which indicate that in the Parkinsonian state, the power curve of STN exhibits a more prominent and narrow spectral peak at 25–30 Hz. Additionally, in Figure 7(f), there exists a sustained, stable, and brighter narrowband stripe around 25 Hz. These phenomena demonstrate markedly elevated β-band oscillation in the STN under Parkinsonian conditions [27].

To provide a direct quantitative comparison between experimental data and the model, two key spectral metrics from STN LFP signals are computed: (i) the peak frequency f_{peak} corresponding to the maximum of the power spectral density (PSD) in the range 1–50 Hz; (ii) R_β is computed as the ratio of the integrated power in the 13–30 Hz band to the total power in the 1–50 Hz range. The results are summarized in Table 3. Both experimental data and the model show that under Parkinsonian conditions, f_{peak} is located within the β-band range, and R_β correspondingly increases.

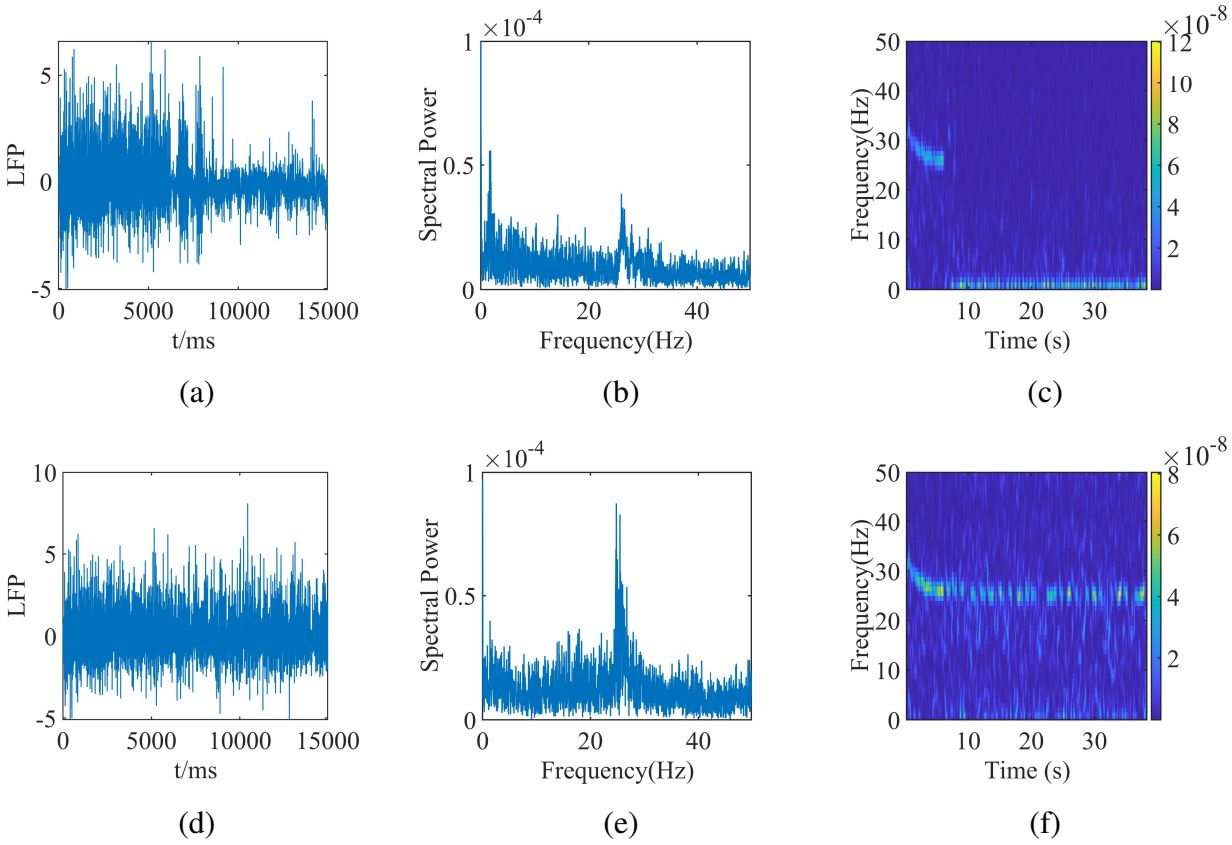

Figure 7. The LFP curves of STN: (a) in healthy condition, (d) in PD. The spectral power of STN neuron: (b) in healthy condition, (e) in PD. The spectral diagram: (c) in healthy condition, (f) in PD.

Table 3. The f_{peak} and R_β of STN.

Conditions	Type	$f_{peak}(Hz)$	R_β
Healthy	Experimental	2.343	0.3972
Parkinsonian	Experimental	26.731	0.5969
Healthy	Model	6.597	0.3047
Parkinsonian	Model	14.99	0.4998

The R_β is calculated as follows:

$$R_\beta = \frac{\int_{13}^{30} P(f)\,df}{\int_{1}^{50} P(f)\,df}, \tag{3.3}$$

where $P(f)$ represents the power spectral density.

β-band synchrony is quantified using two measures: PLV and PC. The PLV is commonly used to assess phase synchrony between two time-series signals. It ranges from 0 to 1, with larger values

reflecting stronger phase synchrony. The calculation formula for the PLV is as follows:

$$\begin{aligned} PLV_{jk} &= \left| \frac{1}{N} \sum_{n=1}^{N} e^{i(\phi_j(n)-\phi_k(n))} \right|, \\ PLV_j &= \frac{1}{S-1} \sum_{k=1}^{S} PLV_{jk} (k \neq j, S > 1), \\ PLV &= \frac{1}{S} \sum_{j=1}^{S} PLV_j, \end{aligned} \tag{3.4}$$

where $\phi_j(n)$and $\phi_k(n)$ represent the instantaneous phase of the signals from the jth and kth neurons, respectively. PLV_{jk} denotes phase synchronization between the signals of the jth and kth neurons. PLV_j denotes the average phase-locking value between the jth neuron and all other neurons within the same nucleus and is used to quantify the network-level phase synchrony of that neuron. The PLV is used to quantify the overall β-band synchrony of the nucleus. In particular, PLV_{jk} is equivalent to PLV_{kj} and $PLV_{jj} = 1$.

Additionally, the PC quantifies the stability of phase relationship between signals within a specified frequency band. The PC ranges from -1 to 1, with positive/negative values indicating in-phase and anti-phase synchrony, respectively. The value near 0 indicates weak or unstable phase relationship. The calculation formula for the PC is as follows [15]:

$$PC_{jk} = \frac{1}{N} \sum_{n=1}^{N} \cos(\phi_j(n) - \phi_k(n)). \tag{3.5}$$

Before computing the PLV and PC, all signals are band-pass filtered in the β-band. Figure 8 analyzes the β-band synchrony from the perspective of single neuron pairs. As can be seen from Figure 8(a)–(c), the phase trajectories of all three neuron-pair types differ markedly, and the phase-difference density distributions are relatively dispersed. By contrast, in the Parkinsonian state, phase trajectories for the same neuron pairs become highly similar, and the phase-difference density distributions become markedly concentrated (see Figures 8(d)–(f)). These findings suggest that, in the pathological state, the β-band synchrony among homologous neuronal pairs in the BG is markedly enhanced.

PLV_j quantifies β-band synchrony at the network level across neurons. The orange column in Figure 9 denotes the healthy condition, whereas the green one indicates the Parkinsonian condition. Specifically, Figures 9(a)–(c) show that, under pathological conditions, the network-level PLV of all three neuronal populations increases markedly, with the STN exhibiting the largest gain.

Figures 10(a)–(c) show that the off-diagonal elements of the PLV matrices for all three nuclei are predominantly light, indicating that, under healthy conditions, the β-band synchrony between neuron pairs within each nucleus is generally weak. In Figures 10(d)–(f), the PLV matrices are overall much darker, with the STN panel being the darkest. This indicates a widespread increase in pairwise β-band phase synchrony within the BG network under pathological conditions, with STN showing the most pronounced enhancement.

Next, this study analyzes the stability of the phase relationship for each neuronal pair. Under healthy conditions, phase synchronization of these three types of nuclei is relatively weak, and most of them are positive (see Figures 11(a)–(c)). In contrast, in the Parkinsonian state (see Figures 11(d)–(f)), there

is a clear distinction between in-phase and anti-phase synchrony, and the overall strength of synchrony is markedly increased. These results clearly indicate that β-band synchrony in the BG is markedly enhanced in the Parkinsonian state.

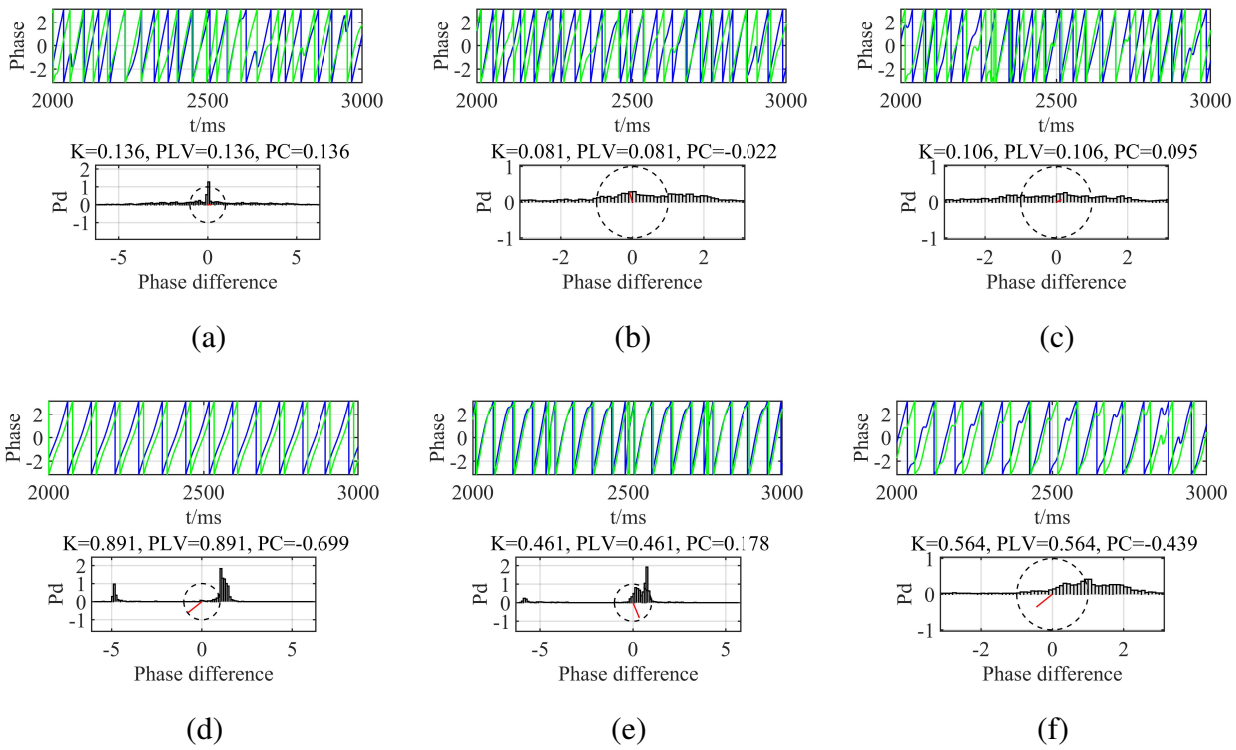

Figure 8. Firing phase diagram of neuronal signal pairs and probability density distribution diagram of phase differences under different conditions. (a) STN in healthy condition. (b) GPe in healthy condition. (c) GPi in healthy condition. (d) STN in PD. (e) GPe in PD. (f) GPi in PD.

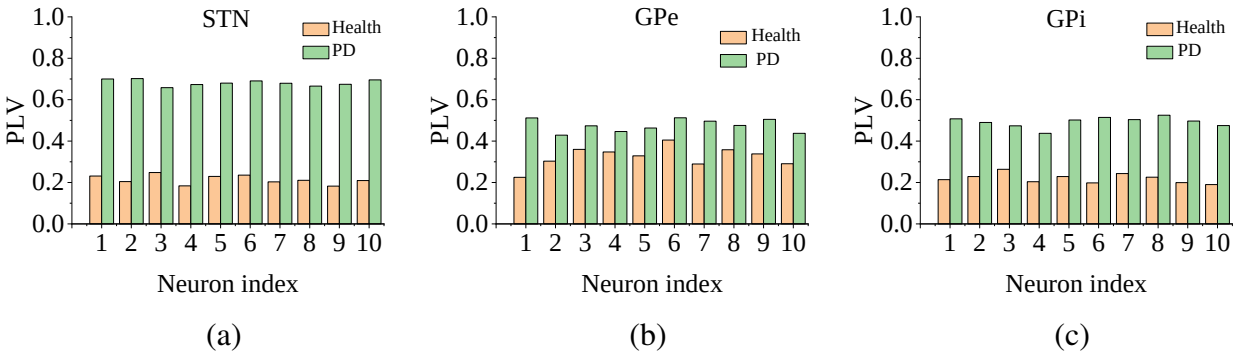

Figure 9. The PLV values of each neuron in different states. (a) STN. (b) GPe. (c) GPi.

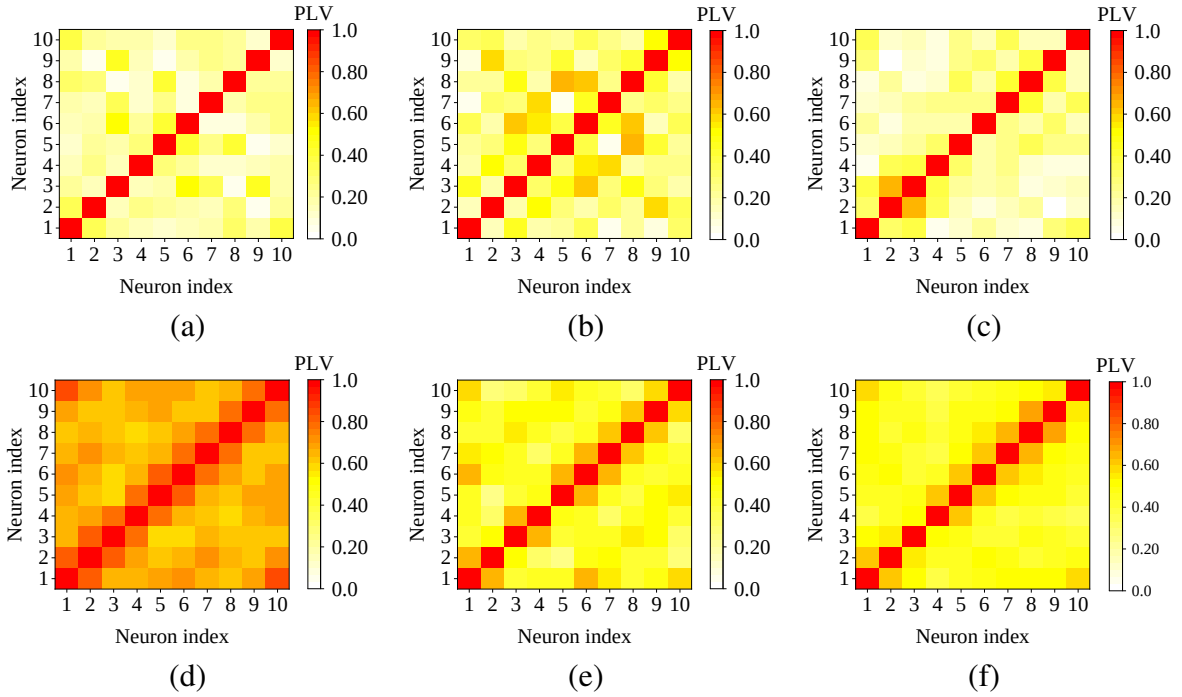

Figure 10. The PLV matrix of each neurons under different conditions. (a) STN in healthy condition. (b) GPe in healthy condition. (c) GPi in healthy condition. (d) STN in PD. (e) GPe in PD. (f) GPi in PD.

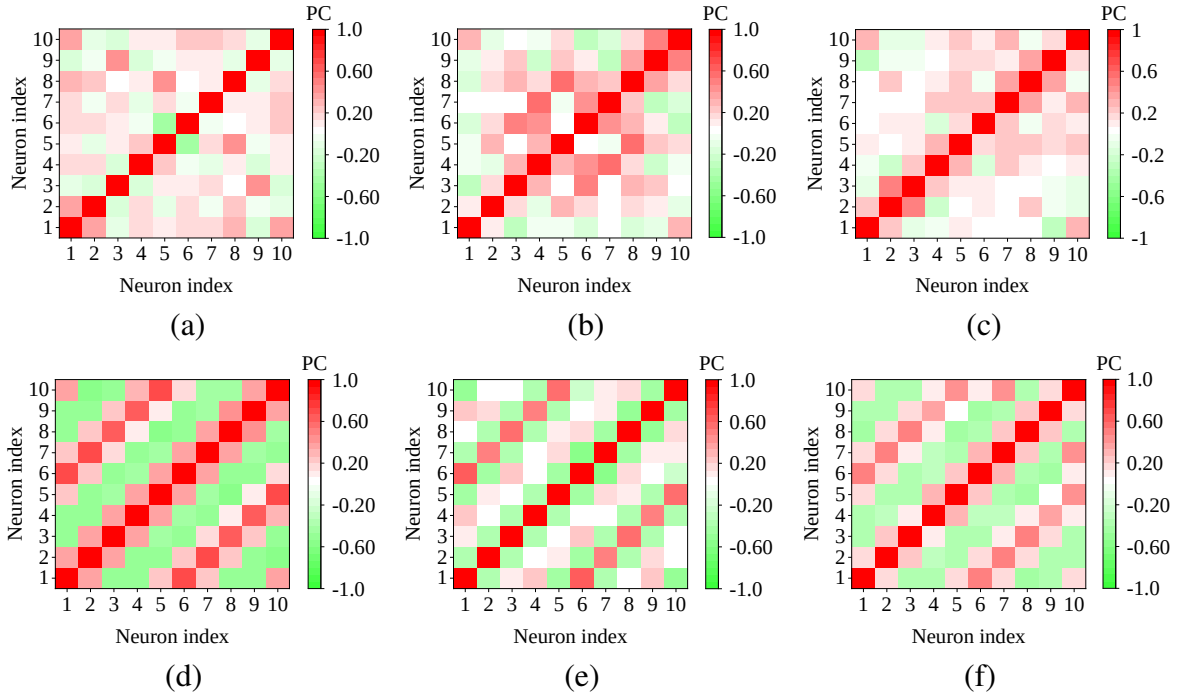

Figure 11. The PC matrix of each neurons under different conditions. (a) STN in healthy condition. (b) GPe in healthy condition. (c) GPi in healthy condition. (d) STN in PD. (e) GPe in PD. (f) GPi in PD.

3.3. Striatal regulation of β-band synchronous oscillations in GPi

As a potential source of network oscillations, the striatum plays a crucial part in generating and transmitting the β-band oscillations. Based on the BGSTC model, we systematically study the striatum's impact on the β-band synchrony within GPi. This is achieved primarily by adjusting the inhibitory synaptic conductances $g_{D1\to GPi}$ and $g_{D2\to GPe}$.

As shown in Figure 12(a), the PLV surface declines as $g_{D1\to GPi}$ increases, indicating that strengthening the striatal inhibition via the direct pathway markedly reduces β-band synchrony among GPi neurons. However, the PLV surface does not change significantly as $g_{D2\to GPe}$ increases. Specifically, it has a synergistic effect on reducing the PLV in the range of $[0.12, 0.14]$ (see Figure 12(b)), but the changes in other larger ranges are not significant or slightly increase. This suggests that strengthening the striatal inhibitory input to GPe via the indirect pathway has a relatively small impact on reducing the β-band synchrony in GPi; it even shows an enhancing trend.

Overall, strengthening striatal inhibition via the direct pathway exerts a stronger "leverage effect" on the β-band desynchronization within GPi. This not only deepens our understanding of the aberrant β-band synchrony in the BG in PD, but also provides a mechanistic basis for therapeutic interventions. To demonstrate that the main conclusions obtained do not depend on the specific value of $Iapp$, the corresponding robustness analysis is provided in the Appendix.

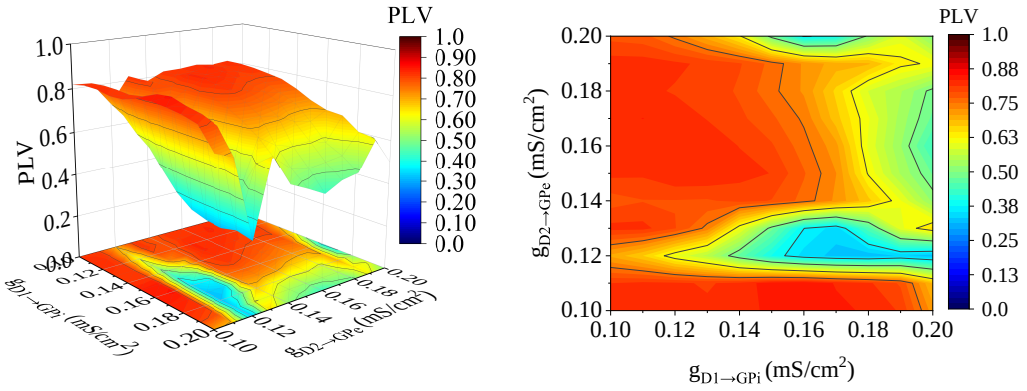

Figure 12. (a) The three-dimensional relationship among $g_{D1\to GPi}$, $g_{D2\to GPe}$ and PLV. (b) The two-dimensional projection at the bottom of (a).

4. Discussion and conclusions

Based on the modified BGSTC framework, this study investigates how striatal inputs modulate the β-band synchrony in GPi from a dynamical-system standpoint. This provides a mechanistic basis for eliminating the pathological β-band synchrony in the BG and emphasizes the importance of the striatum in promoting the β-band desynchronization via the direct pathway.

First, this study simulates the firing activities of the BG under both normal and Parkinsonian conditions. By combining computational simulations with physiological recordings, this study reveals increased β-band oscillations in the BG under Parkinsonian conditions. Next, a hallmark of these abnormal β-band oscillations is a pronounced elevation in synchrony. PLV and PC are used to quantify

pathological β-band synchrony. The results clearly show a pronounced enhancement of the β-band synchrony in the BG under Parkinsonian conditions. Finally, this study systematically analyzes how striatal inputs regulate β-band synchrony in the GPi. These results indicate, compared with the indirect pathway, that striatal inhibitory input to GPi via the direct pathway exerts a stronger effect on the β-band desynchronization.

In summary, within a computational framework, β-band synchrony in the BG is quantified using the PLV and PC, and the effects of striatal inhibitory inputs via the direct and indirect pathways on GPi β-band synchrony are analyzed. These results not only highlight the striatum's critical contribution to the β-band desynchronization in GPi, but they also offer mechanistic support for intervention strategies in PD. At present, the influence of other neurons on the β-band oscillation has not yet been taken into account. In future work, the dynamic effects of other key neuronal populations on neurological disorders will be investigated based on realistic physiological mechanisms.

Use of AI tools declaration

The authors declare they have not used Artificial Intelligence (AI) tools in the creation of this article.

Acknowledgments

This work was supported by the Guangxi Natural Science Foundation (grant number 2025GXNSFAA069751, 2020GXNSFAA297240), the Natural Science Foundation of Guangxi Minzu University (grant number 2022KJQD01), and the National Natural Science Foundation of China (grant number 12062004).

Conflict of interest

The authors declare there are no conflicts of interest.

References

1. Z. Li, X. Shi, B. Bai, The effect of the feedback inhibition of heterogeneous external globus pallidus on beta oscillations in an extended basal ganglia network, *Electron. Res. Arch.*, **33** (2025), 6070–6095. https://doi.org/10.3934/era.2025270
2. J. Jankovic, Parkinson's disease: clinical features and diagnosis, *J. Neurol. Neurosurg. Psychiatry*, **79** (2008), 368–376. https://doi.org/10.1136/jnnp.2007.131045
3. A. Kumar, S. Cardanobile, S. Rotter, A. Aertsen, The role of inhibition in generating and controlling Parkinson's disease oscillations in the basal ganglia, *Front. Syst. Neurosci.*, **5** (2011), 86. https://doi.org/10.3389/fnsys.2011.00086
4. J. E. Rubin, D. Terman, High frequency stimulation of the subthalamic nucleus eliminates pathological thalamic rhythmicity in a computational model, *J. Comput. Neurosci.*, **16** (2004), 211–235. https://doi.org/10.1023/B:JCNS.0000025686.47117.67

5. Y. Guo, J. E. Rubin, C. C. McIntyre, J. L. Vitek, D. Terman, Thalamocortical relay fidelity varies across subthalamic nucleus deep brain stimulation protocols in a data-driven computational model, *J. Neurophysiol.*, **99** (2008), 1477–1492. https://doi.org/10.1152/jn.01080.2007
6. M. M. McCarthy, C. Moore-Kochlacs, X. Gu, E. S. Boyden, X. Han, N. Kopell, Striatal origin of the pathologic beta oscillations in Parkinson's disease, *Proc. Natl. Acad. Sci. U.S.A.*, **108** (2011), 11620–11625. https://doi.org/10.1073/pnas.1107748108
7. A. C. Kreitzer, Physiology and pharmacology of striatal neurons, *Annu. Rev. Neurosci.*, **32** (2009), 127–147. https://doi.org/10.1146/annurev.neuro.051508.135422
8. A. Rădulescu, J. Herron, C. Kennedy, A. Scimemi, Global and local excitation and inhibition shape the dynamics of the cortico-striatal-thalamo-cortical pathway, *Sci. Rep.*, **7** (2017), 7608. https://doi.org/10.1038/s41598-017-07527-8
9. R. So, A. Kent, W. Grill, Relative contributions of local cell and passing fiber activation and silencing to changes in thalamic fidelity during deep brain stimulation and lesioning: a computational modeling study, *J. Comput. Neurosci.*, **32** (2012), 499–519. https://doi.org/10.1007/s10827-011-0366-4
10. S. J. van Albada, P. A. Robinson, Mean-field modeling of the basal ganglia-thalamocortical system. I: Firing rates in healthy and parkinsonian states, *J. Theor. Biol.*, **257** (2009), 642–663. https://doi.org/10.1016/j.jtbi.2008.12.018
11. A. H. Gittis, G. B. Hang, E. S. LaDow, L. R. Shoenfeld, B. V. Atallah, S. Finkbeiner, et al., Rapid target-specific remodeling of fast-spiking inhibitory circuits after loss of dopamine, *Neuron*, **71** (2011), 858–868. https://doi.org/10.1016/j.neuron.2011.06.035
12. V. L. Corbit, T. C. Whalen, K. T. Zitelli, S. Y. Crilly, J. E. Rubin, A. H. Gittis, Pallidostriatal projections promote β oscillations in a dopamine-depleted biophysical network model, *J. Neurosci.*, **36** (2016), 5556–5571. https://doi.org/10.1523/JNEUROSCI.0339-16.2016
13. L. di Biase, L. Ricci, M. L. Caminiti, P. M. Pecoraro, S. P. Carbone, V. Di Lazzaro, Quantitative high density EEG brain connectivity evaluation in Parkinson's disease: the phase locking value (PLV), *J. Clin. Med.*, **12** (2023), 1450. https://doi.org/10.3390/jcm12041450
14. J. J. Jui, I. T. Hettiarachchi, A. Bhatti, D. Creighton, PLVNet: EEG-based trust classification using phase locking value connectivity and deep neural networks, *Comput. Biol. Med.*, **198** (2025), 111269. https://doi.org/10.1016/j.compbiomed.2025.111269
15. M. Vinck, M. van Wingerden, T. Womelsdorf, P. Fries, C. M. A. Pennartz, The pairwise phase consistency: a bias-free measure of rhythmic neuronal synchronization, *NeuroImage*, **51** (2010), 112–122. https://doi.org/10.1016/j.neuroimage.2010.01.073
16. M. Galarreta, S. Hestrin, Electrical synapses between GABA-releasing interneurons, *Nat. Rev. Neurosci.*, **2** (2001), 425–433. https://doi.org/10.1038/35077566
17. Y. Yu, Q. Wang, Oscillation dynamics in an extended model of thalamic-basal ganglia, *Nonlinear Dyn.*, **98** (2019), 1065–1080. https://doi.org/10.1007/s11071-019-05249-2
18. E. Charyasz, M. Erb, J. Bause, R. Heule, B. Bender, V. K. Jangir, et al., Functional connectivity of thalamic nuclei during sensorimotor task-based fMRI at 9.4 Tesla, *Front. Neurosci.*, **19** (2025), 1568222. https://doi.org/10.3389/fnins.2025.1568222

19. P. L. Chen, Y. C. Chen, P. H. Tu, T. C. Liu, M. C. Chen, H. T. Wu, et al., Subthalamic high-beta oscillation informs the outcome of deep brain stimulation in patients with Parkinson's disease, *Front. Hum. Neurosci.*, **16** (2022), 958521. https://doi.org/10.3389/fnhum.2022.958521

20. F. Su, M. Chen, L. Zu, S. Li, H. Li, Model-based closed-loop suppression of Parkinsonian beta band oscillations through origin analysis, *IEEE Trans. Neural Syst. Rehabil. Eng.*, **29** (2021), 450–457. https://doi.org/10.1109/TNSRE.2021.3056544

21. E. M. Radcliffe, A. J. Baumgartner, D. S. Kern, M. Al Borno, S. Ojemann, D. R. Kramer, et al., Oscillatory beta dynamics inform biomarker-driven treatment optimization for Parkinson's disease, *J. Neurophysiol.*, **129** (2023), 1492–1504. https://doi.org/10.1152/jn.00055.2023

22. T. Hodnik, S. Roytman, N. I. Bohnen, U. Marusic, Beta-gamma phase-amplitude coupling as a non-invasive biomarker for Parkinson's disease: insights from electroencephalography studies, *Life(Basel)*, **14** (2024), 391. https://doi.org/10.3390/life14030391

23. P. Brown, D. Williams, Basal ganglia local field potential activity: character and functional significance in the human, *Clin. Neurophysiol.*, **116** (2005), 2510–2519. https://doi.org/10.1016/j.clinph.2005.05.009

24. C. Xing, X. Cheng, H. Feng, B. Wu, Y. Nie, C. Chu, et al., A real-time artifact removal system for closed-loop deep-brain stimulation, *IEEE Trans. Neural Syst. Rehabil. Eng.*, **33** (2025), 3237–3245. https://doi.org/10.1109/TNSRE.2025.3597916

25. X. Wang, Y. Yu, F. Han, Q. Wang, Dynamical mechanism of parkinsonian beta oscillation in a heterogeneous subthalamopallidal network, *Nonlinear Dyn.*, **111** (2023), 10505–10527. https://doi.org/10.1007/s11071-023-08381-2

26. A. Biswas, H. An, Preliminary results of neuromorphic controller design and a Parkinson's disease dataset building for closed-loop deep brain stimulation, preprint, arXiv:2407.17756.

27. J. Li, L. Wang, Y. Pan, P. Huang, L. Xu, Y. Zhang, et al., Subthalamic nucleus oscillations during facial emotion processing and apathy in Parkinson's disease, *J. Affect. Disord.*, **373** (2025), 314–324. https://doi.org/10.1016/j.jad.2025.01.005

Appendix

To examine whether the main conclusions depend on the specific applied-current values used to define the Parkinsonian state, the $Iapp$ data reported in the work of So et al. (Table A1) are used to repeat the key analyses. The main quantitative findings remains unchanged across both Parkinsonian $Iapp$ parameter sets: (i) under Parkinsonian conditions, the pairwise synchrony among GPi neurons is markedly enhanced (Figure A1), with a clear separation between in-phase and anti-phase (Figure A2); (ii) as $g_{D1\to GPi}$ increases, the synchrony level in the GPi shows a decreasing trend (Figure A3).

Table A1. The $Iapp$ reported in the work of So et al.

Conditions	I_{app}^{STN}	I_{app}^{GPe}	I_{app}^{GPi}
Healthy	$33\mu A/cm^2$	$20\mu A/cm^2$	$21\mu A/cm^2$
Parkinsonian	$23\mu A/cm^2$	$7\mu A/cm^2$	$15\mu A/cm^2$

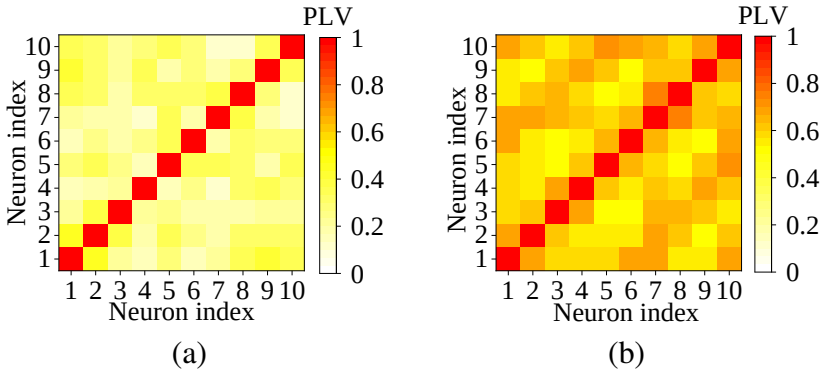

Figure A1. The PLV matrix of GPi under different conditions: (a) Healthy. (b) PD.

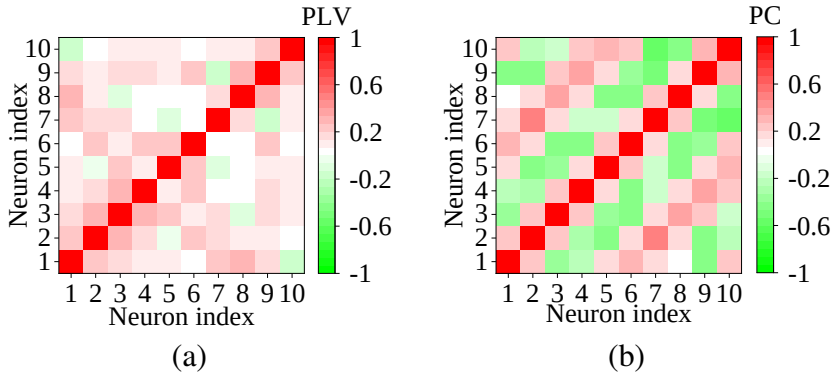

Figure A2. The PC matrix of GPi under different conditions: (a) Healthy. (b) PD.

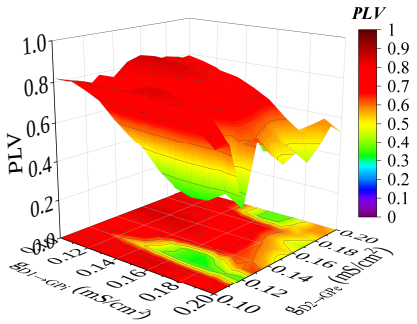

Figure A3. The three-dimensional relationship diagram among $g_{D1\to GPi}$, $g_{D2\to GPe}$ and PLV.